Updated regional precipitation and temperature changes for the 21st century from ensembles of recent AOGCM simulations

F. Giorgi and X. Bi

Abdus Salam International Centre for Theoretical Physics, Trieste, Italy

Received 3 August 2005; revised 20 September 2005; accepted 10 October 2005; published 11 November 2005.

[1] We present an analysis of regional precipitation and temperature changes for different 20-year periods (20 yrp) of the 21st century from the latest ensemble of global model simulations (20 models) over 26 land regions worldwide and 3 IPCC emission scenarios (A1B, A2, B1). We find that regional warming enhancements and precipitation changes are mostly in agreement with previous generation models (with some notable exceptions). A high level of agreement of weighted ensemble average regional changes is found across scenarios and across different periods within the 21st century. Overall, both for temperature and precipitation, the dry seasons appear generally more responsive to GHG forcing than the wet seasons. Our results indicate that the precipitation and temperature change projections produced by ensembles of current global model simulations show increasingly consistent regional patterns. **Citation:** Giorgi, F., and X. Bi (2005), Updated regional precipitation and temperature changes for the 21st century from ensembles of recent AOGCM simulations, *Geophys. Res. Lett.*, *32*, L21715, doi:10.1029/2005GL024288.

1. Introduction

[2] In a previous paper, *Giorgi et al.* [2001, hereinafter referred to as G01] reported on regional temperature and precipitation mean changes for the last decades of the 21st century from an ensemble of 9 coupled Atmosphere-Ocean General Circulation Model (AOGCM) simulations. G01 considered 22 land regions of the globe and the A2 and B2 *Intergovernmental Panel on Climate Change* (*IPCC*) [2001] greenhouse gas (GHG) and aerosol emission scenarios. Since then, a larger number of modeling groups completed a new set of transient climate change simulations. This offers the opportunity to re-evaluate on stronger grounds model-based projections of regional climate changes.

[3] Here we present regional changes in precipitation and surface air temperature from this latest generation of AOGCM simulations. Our results can be broadly compared with those of G01, but some important differences need to be emphasized: 1) While G01 focused on the summer and winter seasons, we divide the year into two six-month periods, a "wet season" and a "dry season" (or for some regions two different rainy seasons); this allows us to cover the entire year and to choose more targeted sub-annual partitions for the different regions; 2) G01 considered the future period 2071–2100, while we examine the 5 consecutive 20 yrp of the 21 century, which allows us to address issues of multidecadal variability and trends; 3) While G01 presented results on intermodel agreement of projections, we focus on multi-model averaged changes based on the Reliability Ensemble Averaging (REA) method of *Giorgi and Mearns* [2002, hereinafter referred to as GM02]; 4) Our regional partitioning of the globe's land areas is slightly different from that of G01; 5) We analyze three IPCC emission scenario, A1B, A2 and B1; of these, B1 is close to the lower end of the IPCC scenario range, A2 is close to the upper end and A1B lies towards the middle of the range.

2. Methodology

[4] Gridded global monthly surface air temperature and precipitation for the simulations are obtained from the Program for Climate Model Diagnosis and Intercomparison (PCMDI, http://www-pcmdi.llnl.gov). All experiments include monthly data for 1901–1999 and 2000–2099 for at least one scenario (Table 1). For some models multiple realizations are available and in these cases we use the ensemble average of the realizations.

[5] Because the models utilize different horizontal grids, for intercomparison purposes we interpolate the model data onto a common global 1 degree grid. A corresponding 1 degree land mask grid is obtained from a fine scale vegetation dataset. Twenty-six regions are then defined (Table 2 and Figure 1) and the model data are averaged over the land points within each region based on this land mask grid. Because of the different land configurations in the models this procedure generates some uncertainty over coastal areas. Note that our regions slightly differ from those of G01 (e.g. in Africa and South America). The monthly regional values are aggregated over two six-month periods defining a "wet season" and a "dry season" (or alternatively two different rainy seasons) for each region based on observed climatologies of monthly precipitation (Table 2).

[6] We analyze differences, or "changes", in mean fields between the five 20 yrp of the 21st century (2000–2019, 2020–2039, 2040–2059, 2060–2079, 2080–2099) and the reference period 1960–1979, i.e. a recent climate period characterized by a relatively small anthropogenic component [*IPCC*, 2001]. We calculate ensemble average changes across models using the REA method of GM02 in which however the reliability parameter depends only on the model bias and not on the model spread (see equations 3 and 4 of GM02). We therefore do not utilize the model convergence criterion of GM02. The model biases and natural variability estimates necessary to calculate the REA weights (see GM02) are computed using observations

0094-8276/05/2005GL024288

Table 1. List of Models and Simulations Used in the Analysis[a]

Model	20 Cent.	A1B	A2	B1
BCCR-BCM2-0	1	-	1	1
CCMA-3-T47	5	4	2	4
CNRM-CM3	1	1	1	1
CSIRO-MK3	2	1	1	1
GFDL-CM2-0	3	1	1	1
GFDL-CM2-1	3	1	1	-
GISS-AOM	2	2	-	2
GISS-EH	5	4	-	-
GISS-ER	1	2	1	1
IAP-FGOALS	3	3	-	2
INMCM3	1	1	1	1
IPSL-CM4	1	1	1	1
MIROC3-2H	1	1	-	1
MIROC3-2M	3	3	3	3
MIUB-ECHO-G	5	3	3	3
MPI-ECHAM5	3	2	3	3
MRI-CGCM2	5	5	5	5
NCAR-CCSM3	8	6	4	8
NCAR-PCM1	4	3	4	2
UKMO-HADCM3	1	1	1	1

[a]See the PCMDI web site for more information on the models.

from the Climatic Research Unit (CRU) dataset. Table 3 shows examples of regional precipitation biases. When averaged across models, they are mostly lower than 50%, but they also show a large inter-model spread. In some sense, this justifies the use of performance weighting in the ensemble averaging. For temperature (not shown) the ensemble average biases are mostly less than 2°C while the biases for individual models can exceed 6–8°C.

3. Results

[7] Figure 1 shows the REA change in wet season and dry season precipitation and temperature for each region and for the three scenarios. The corresponding ensemble average global changes (including ocean areas) in annual surface air temperature and precipitation are shown in Table 4. The histograms in Figure 1 indicate the precipitation changes for the A1B scenario, while the vertical bars denote the range obtained when including also the REA average A2 and B1 changes (the A2 being the most extreme in almost all cases). In general, regional temperature changes scale well with the global temperature change, therefore for each region we report as a colored square the ratio of the REA regional temperature change to the ensemble average global change. This ratio is referred to as Regional Warming Amplification Factor, or RWAF, and it is obtained by averaging the RWAF obtained for the five 20 yrp in the 21st century and the three scenarios. In fact, RWAF varies by less than 15–20% across different 20 yrp and scenarios.

[8] The global warming (Table 4) is highest for the A1B scenario in the first three 20 yrp of the century, while it accelerates and becomes maximum in the A2 scenario during the last two 20 yrp. This behavior is tied to the temporal evolution of GHG emissions (greater in A1B than A2 up to about 2030 and lower afterwards [*IPCC*, 2001]) and the forcing-temperature response lag. The B1 scenario shows the lowest global warming in all 20 yrp except the first. All the regional temperature changes have the same temporal evolution as the global temperature change and most regional land areas warm more than the global average, with RWAF values of up to 2. As in G01, the largest RWAFs are found in high latitude northern hemisphere regions. Also, for the majority of regions the RWAF is greater in the dry season than the wet season, regardless of whether the dry season is also the colder one and regardless of the sign of the precipitation change. In

Table 2. Definition of "Wet Season" and "Dry Season" for the Regions in Figure 1[a]

Region	Lat; Lon	Wet Season	Dry Season
NEU	47–70 N; 10.5 W–27.5 E	May–Oct. (2.3; 12.2)	Nov.–Apr. (1.8; −0.3)
MED	30–47 N; 10.5 W–37.5 E	Oct.–Mar. (1.8; 8.9)	Apr.–Sept. (1.2; 19.7)
NEE	47–70 N; 27.5–60.5 E	May–Oct. (1.7; 12.8)	Nov.–Apr. (1.2; −6.1)
NAS	47–70 N; 60.5–180.5 E	May–Oct. (1.7; 7.6)	Nov.–Apr. (0.6; −19.5)
CAS	30–47 N; 37.5–80.5 E	Nov.–Apr. (1.1; 3.9)	May–Oct. (0.6; 20.3)
TIB	30–47 N; 80.5–104.5 E	Apr.–Sept. (1.1; 10.5)	Oct.–Mar. (0.2; −7.2)
EAS	20–47 N; 104.5–140.5 E	Apr.–Sept. (3.8; 19.1)	Oct.–Mar. (1.1; 2.0)
SAS	5–30 N; 104.5–140.5 E	May–Oct. (6.1; 25.6)	Nov.–Apr. (0.8; 19.6)
SEA	10 S–20 N; 100.5–150.5 E	Apr.–Sept. (7.2; 25.7)	Oct.–Mar. (7.0; 25.0)
NAU	28–10 S; 109.5–155.5 E	Nov.–Apr. (2.5; 27.8)	May–Oct. (0.5; 19.8)
SAU	45–28 S; 109.5–155.5 E	May–Oct. (1.2; 13.1)	Nov.–Apr. (1.1; 21.9)
SAH	18–30 N; 20.5 W–65.5 E	Nov.–Apr. (0.2; 19.0)	May–Oct. (0.1; 29.6)
WAF	0–18 N; 20.5 W–20.5 E	May–Oct. (4.6; 27.5)	Nov.–Apr. (0.98; 26.3)
EAF	0–18 N; 20.5–52.5 E	May–Oct. (3.0; 25.9)	Nov.–Apr. (0.9; 24.1)
EQF	8 S–4 N; 28.5–43.5 E	Feb.–July (2.7; 23.0)	Aug.–Jan. (2.4; 23.0)
SQF	26–0 S; 0.5–55.5 E	Nov.–Apr. (4.9; 23.7)	May–Oct. (1.1; 20.6)
SAF	35–26 S; 9.5–40.5 E	Oct.–Mar. (1.7; 21.0)	Apr.–Sept. (0.7; 13.3)
ALA	50–87 N; 179.5–103.5 W	June–Nov. (1.5; 3.3)	Dec.–May (0.9; −13.3)
GRL	50–87 N; 103.5–12.5 W	June–Nov. (1.8; −2.3)	Dec.–May (1.1; −18.8)
WNA	30–50 N; 129.5–103.5 W	Oct.–Mar. (1.5; 2.8)	Apr.–Sept. (1.1; 15.7)
CNA	30–50 N; 103.5–85.5 W	Apr.–Sept. (2.8; 19.6)	Oct.–Mar. (1.7; 3.1)
ENA	25–50 N; 85.5–60.5 W	Apr.–Sept. (3.2; 16.3)	Oct.–Mar. (2.7; 0.7)
CAM	12–30 N; 120.5–83.5 W	May–Oct. (4.6; 24.0)	Nov.–Apr. (1.1; 18.5)
AMZ	20 S–10 N; 78.5–34.5 W	Nov.–Apr. (6.3; 24.9)	May–Oct. (4.0; 24.1)
CSA	40–20 S; 78.5–34.5 W	Oct.–Mar. (3.2; 20.6)	Apr.–Sept. (1.7; 14.0)
SSA	56–40 S; 78.5–34.5 W	Apr.–Sept. (1.8; 4.5)	Oct.–Mar. (1.1; 11.7)

[a]The average observed precipitation (mm/day) and temperature (°C) for each season and region and for the 20 yrp 1960–1979 are reported in parentheses, respectively.

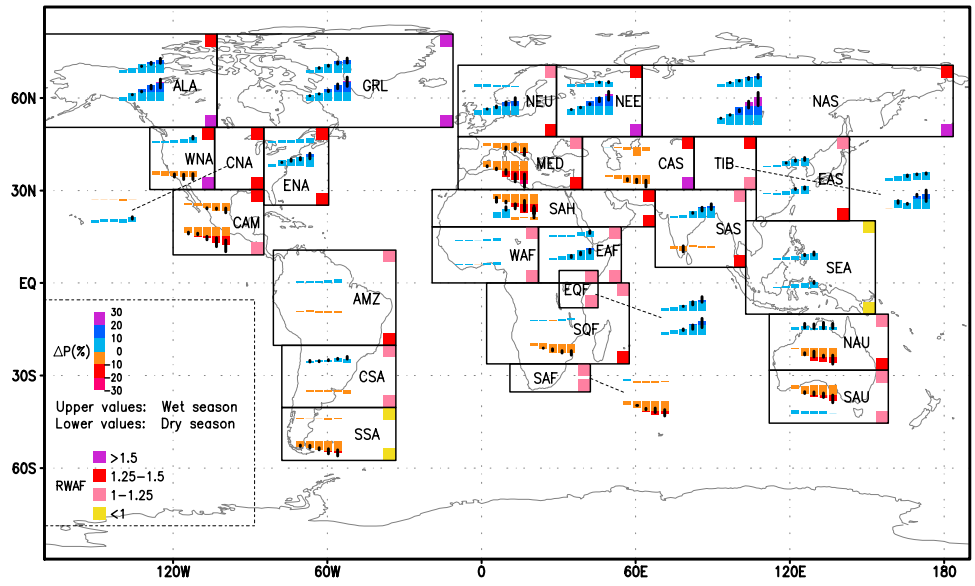

Figure 1. REA precipitation and temperature changes for the "wet season" and "dry season" over 26 land regions of the world (see Table 2). The histograms present precipitation changes for the 20 yrp 2000–2019, 2020–2039, 2040–2059, 2060–2079, 2080–2099 with respect to 1960–1979 in the A1B scenario. The black vertical bars present the range obtained when considering also the A2 and B1 scenarios (shown only for changes exceeding 5%). Units are % of 1960–1979 precipitation. The squares present the regional warming amplification factor (RWAF), i.e. the ratio of the REA regional warming over the corresponding ensemble average global warming. The RWAF values shown are calculated by averaging RWAF over all 20 yrp and all three scenarios. For both the precipitation histograms and the RWAF squares, upper values are for the wet season and lower values are for the dry season.

other words, regional temperatures are more responsive to the GHG forcing in the dry season than the wet season.

[9] The regional precipitation changes show that in most cases the sign of the REA change does not reverse at multi-decadal scales, but rather it tends to intensify with time so that a well defined trend occurs throughout the century. Ensemble averaging filters out multidecadal variability of individual realizations and therefore is indicative of general trends. In reality, however, future climate would be only one realization of all possible futures and as such it would show

Table 3. Regional Precipitation Ensemble Average Biases (1960–1979) and REA Changes ([2070–2099] Minus [1960–1979]) for the A1B Acenario[a]

Region	P-Bias WS	P-Change WS	P-Bias DS	P-Change DS
NEU	−3.5 (−34.8; 17.2)	1.0 (−14.3; 18.5)	21.2 (−9.0; 59.8)	**14.4** (3.5; 22.5)
MED	−10.5 (−25.5; 27.1)	**−10.3** (−21.9; 1.5)	−8.5 (−50.4; 38.2)	**−23.2** (−8.1; −45.4)
NEE	−10.0 (−57.4; 29.6)	**6.0** (−9.3; 25.5)	23.9 (−14.7; 85.9)	**20.9** (11.6; 33.8)
NAS	12.1 (−29.5; 46.4)	**11.6** (1.2; 21.1)	42.6 (−7.3; 131.0)	**28.3** (15.0; 48.8)
CAS	16.8 (−29.1; 51.6)	−1.8 (−10.8; 8.1)	15.1 (−30.4; 106.8)	**−10.5** (−29.3; 18.0)
TIB	105.4 (39.2; 201.3)	**8.5** (−1.8; 33.2)	310.1 (93.9; 919.7)	**14.9** (4.2; 46.0)
EAS	2.8 (−17.6; 20.0)	**8.5** (−1.9; 17.7)	43.3 (−19.6; 120.3)	**7.8** (−8.5; 26.5)
SAS	−18.9 (−63.6; 10.2)	**11.1** (−6.5; 26.1)	31.2 (−28.4; 88.1)	−2.2 (−28.2; 13.2)
SEA	−6.0 (−34.5; 28.8)	**7.2** (−1.8; 18.9)	−3.8 (−39.9; 34.2)	**6.0** (−0.9; 19.7)
NAU	15.1 (−76.0; 117.5)	1.9 (−25.5; 26.8)	44.2 (−54.3; 218.1)	**−13.2** (−53.6; 24.2)
SAU	−4.9 (−60.4; 42.5)	**−13.5** (−26.9; 8.4)	18.4 (−55.7; 101.8)	0.4 (−25.7; 26.6)
SAH	−26.8 (−74.3; 83.6)	**−17.8** (−28.1; 0.3)	137.3 (−91.8; 287.2)	−5.7 (−53.7; 83.8)
WAF	−3.9 (−47.7; 36.4)	1.2 (−16.1; 15.5)	22.6 (−23.3; 88.4)	1.5 (−12.2; 16.9)
EAF	15.1 (−40.5; 84.3)	**5.3** (−13.2; 19.7)	45.4 (−26.3; 99.8)	**11.8** (−8.5; 26.3)
EQF	3.5 (−44.2; 56.9)	**11.7** (−8.3; 34.1)	46.0 (3.1; 103.0)	**13.4** (1.5; 49.3)
SQF	9.5 (−28.4; 33.0)	1.86 (−5.3; 8.8)	32.9 (−14.7; 68.5)	−6.7 (−20.1; 10.3)
SAF	54.1 (−30.5; 182.6)	−0.9 (−19.2; 16.4)	77.3 (−9.8; 205.7)	**−12.4** (−24.6; 8.4)
ALA	46.4 (23.6; 80.7)	**13.8** (3.8; 26.2)	73.5 (31.2; 163.7)	**19.9** (4.9; 32.2)
GRL	−2.2 (−13.6; 25.2)	**14.4** (8.5; 26.8)	2.4 (−29.0; 53.8)	**20.8** (4.2; 32.2)
WNA	46.8 (−1.56; 115.6)	4.9 (−3.9; 24.6)	46.5 (−2.3; 118.5)	**−6.1** (−19.3; 9.5)
CNA	−0.9 (−25.1; 34.3)	−0.84 (−27.0; 22.8)	6.13 (−19.3; 65.9)	4.7 (−12.3; 14.3)
ENA	1.3 (−14.1; 28.6)	**4.5** (−13.0; 14.9)	2.6 (−22.9; 28.4)	**12.0** (1.3; 24.7)
CAM	−18.7 (−62.6; 23.5)	**−10.1** (−47.0; 11.4)	66.1 (−12.1; 233.3)	**−18.2** (−53.5; 1.2)
AMZ	−13.3 (−31.2; 15.7)	3.8 (−12.6; 15.6)	−30.3 (−61.5; 9.4)	−1.2 (−36.4; 12.5)
CSA	−0.2 (−50.8; 33.6)	3.2 (−22.1; 13.3)	−19.4 (−51.7; 15.3)	−2.6 (−24.3; 27.3)
SSA	85.7 (30.6; 117.0)	−0.5 (−7.6; 9.5)	169.5 (87.4; 251.5)	**−10.2** (−19.9; −2.4)

[a]In parentheses are the corresponding ranges of values found for individual models within the ensemble. Units are %; WS is wet season, DS is dry season. Bold values indicate that at least 80% of the models agree on the sign of the change.

Table 4. Ensemble Average Global Temperature (T, °C) and Precipitation (P, %) Change (With Respect to 1960–1979) for Three IPCC Emission Scenarios

Scenario	2000–2019	2020–2039	2040–2059	2060–2079	2080–2099
			T-Change		
A1B	0.725	1.211	1.817	2.314	2.850
A2	0.708	1.116	1.709	2.498	3.384
B1	0.715	1.078	1.428	1.814	2.042
			P-Change		
A1B	1.049	1.664	2.629	3.743	4.578
A2	1.057	1.431	2.256	3.623	5.067
B1	1.068	1.582	2.172	3.030	3.652

substantial interdecadal variability that should be taken into account when developing scenarios for use in impact studies [*Giorgi*, 2005]. Figure 1 also shows that when the precipitation change is large, an agreement across scenarios is generally found. Similarly to temperature, also for precipitation the dry seasons tend to be more responsive than the wet seasons to GHG forcings (with some exceptions, e.g. the Asia Monsoon seasons).

[10] As in G01, high latitude northern hemisphere regions show the largest increases in precipitation (up to 20% or more), particularly during the drier (winter) seasons. Precipitation decreases in both the wet and dry seasons are found over the Central America (CAM), Mediterranean (MED) and Central Asia (CAS) regions. The results for CAS and MED in the wet (winter) season are somewhat in contrast to those of G01, which showed increasing precipitation over CAS and no strong signal over the MED in winter. As in G01, an increase in monsoon precipitation is found over the East Asia (EAS), South Asia (SAS) and Southeast Asia (SEA) regions.

[11] Small precipitation changes occur over West Africa (WAF), while increased precipitation in both the long rain and short rain seasons are projected over the East Africa (EAF) and East Equatorial Africa (EQF) regions. A decrease of precipitation in the local winter seasons is found over the southernmost regions of the southern hemisphere, which has been attributed to a southward shift of the mid-latitude storm track (G01). Precipitation decreases for the Northern Australia (NAU) dry season (winter) and the Sahara (SAH) wet season (winter).

[12] Finally, Figure 1 shows only small precipitation changes over the Amazon (AMZ) and Central South America (CSA). Over Western North America (WNA), precipitation increases in the wet season (winter) and decreases in the dry season (summer), thereby enhancing the seasonal precipitation cycle. Small changes are projected over Central North America (CNA), while an increase in dry season (winter) precipitation occurs over Eastern North America (ENA).

[13] Table 3 shows examples of inter-model spread of precipitation changes for the last 20 yrp of the A1B scenario, indicating that this spread is still generally large. However, over regions where the REA change exceeds 5% there is a good inter-model agreement of the sign of the simulated change.

4. Conclusions

[14] Our main conclusions are the following:

[15] 1) The latest generation models show regional warming enhancements and precipitation changes that are mostly in agreement with previous generation models [*Kittel et al.*, 1998; G01], with some noticeable exceptions (e.g. CAS, SAH, and MED in winter).

[16] 2) A high level of agreement of REA regional changes (both for temperature and precipitation) is found across scenarios. Over regions where the REA precipitation changes are largest, these tend to keep the same sign and intensify during the 21st century. For these cases a good inter-model agreement in the sign of the simulated change is found.

[17] 3) Overall, both for temperature and precipitation the dry seasons appear more responsive to GHG forcing than the wet seasons (with some exceptions, e.g the Asia monsoon seasons).

[18] Conclusions 1) and 2) above indicate that the precipitation and temperature change projections produced by ensembles of simulations with current models are showing increasingly consistent regional patterns. We stress that ensemble averaging filters out interdecadal variability and, particularly for precipitation, this should be taken into account when developing regional climate change scenarios suitable for impact studies [*Giorgi*, 2005]. We are currently carrying out a more detailed regional analysis of these simulations, including aspects of interannual variability and extremes to report in more extended forthcoming papers.

References

Giorgi, F. (2005), Interdecadal variability of regional climate change: Implications for the development of regional climate change scenarios, *J. Meteorol. Atmos. Phys.*, *89*, 1–15.

Giorgi, F., and L. O. Mearns (2002), Calculation of average, uncertainty range and reliability of regional climate changes from AOGCM simulations via the "Reliability Ensemble Averaging (REA)" method, *J. Clim.*, *15*, 1141–1158.

Giorgi, F., P. W. Whetton, R. G. Jones, J. H. Christensen, L. O. Mearns, B. Hewitson, H. vonStorch, R. Francisco, and C. Jack (2001), Emerging patterns of simulated regional climatic changes for the 21st century due to anthropogenic forcings, *Geophys. Res. Lett.*, *28*, 3317–3320.

Intergovernmental Panel on Climate Change (2001), *Summary for Policy Makers and Technical Summary of the Working Group I Report*, 98 pp., Cambridge Univ. Press, New York.

Kittel, T. G. F., F. Giorgi, and G. A. Meehl (1998), Intercomparison of regional biases and doubled CO2 sensitivity of coupled atmosphere-ocean general circulation model experiments, *Clim. Dyn.*, *14*, 1–15.

X. Bi and F. Giorgi, Abdus Salam International Centre for Theoretical Physics, I-34014 Trieste, Italy. (bixq@ictp.it; giorgi@ictp.it)